Supplementary data for

Acridine-based macrocyclic fluorescent sensors: self-assembly behavior characterized by crystal structures and tunable bathochromic-shift in emission induced by $H_2PO_4^-$ via adjusting the ring size and rigidity

Dawei Zhang,[a] Xiaozhi Jiang,[a] Haiqiang Yang,[a] Alexandre Martinez,*[b] Meiyun Feng,[a] Zhiyun Dong[a] and Guohua Gao*[a]

[a]*Shanghai Key Laboratory of Green Chemistry and Chemical Processes, Department of Chemistry, East China Normal University, 3663 North Zhongshan Road, Shanghai, 200062, P. R. China. Tel and Fax: +86(21)62233323, ghgao@chem.ecnu.edu.cn*

[b]*Laboratoire de Chimie, CNRS, École Normale Supérieure de Lyon, 46, Allée d'Italie, F-69364, Lyon, France. E-mail: alexandre.martinez@ens-lyon.fr*

Graphical abstract

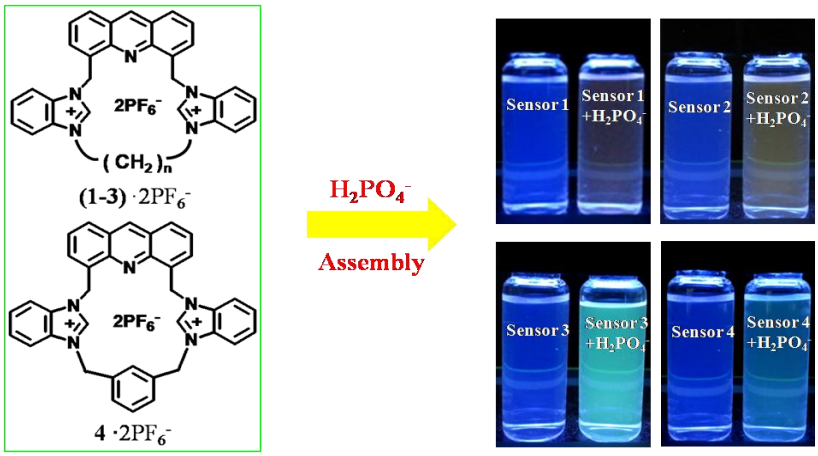

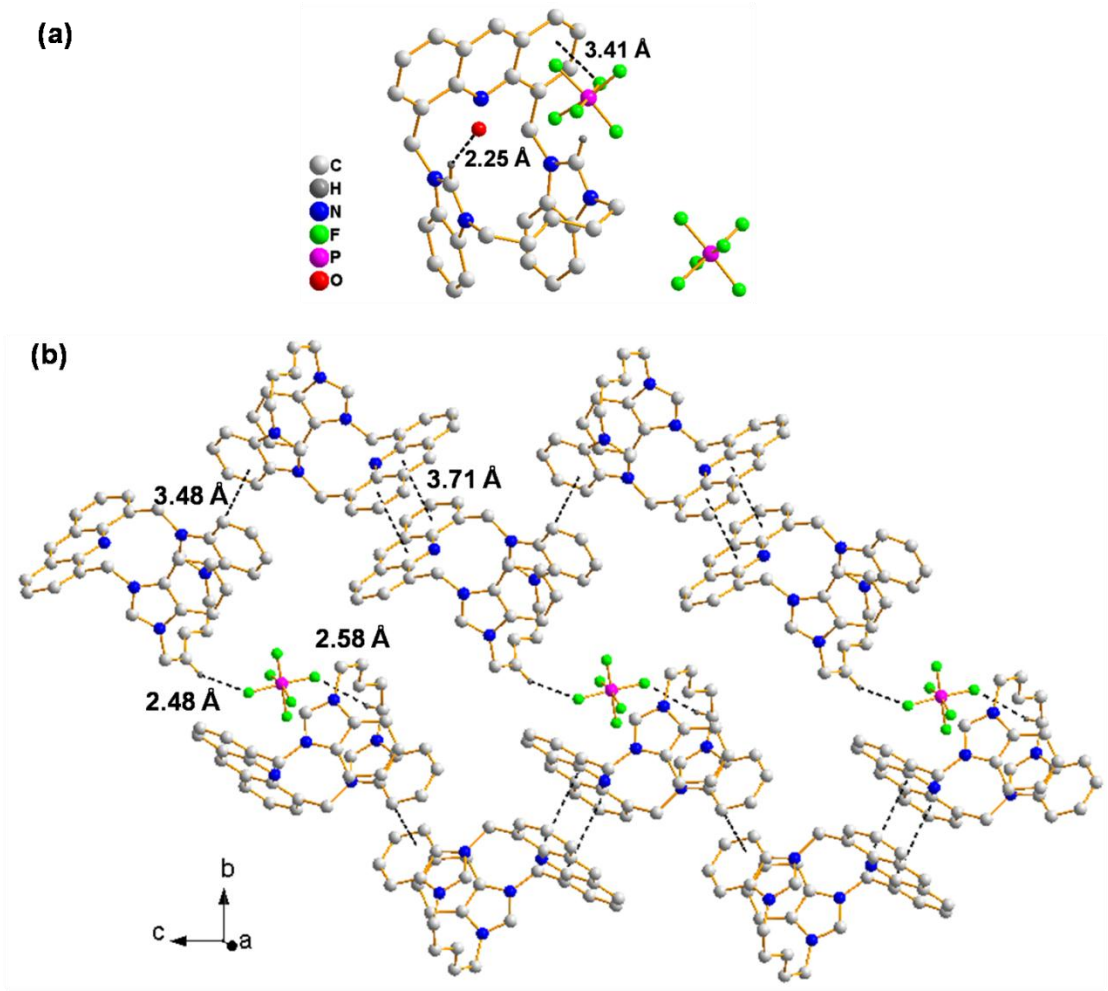

Fig. **S1** Crystal structure (a) and the self-assembly network (b) of **2**·2(PF_6^-)·0.5(H_2O). Nonacidic hydrogen atoms, some counterions and solvent molecules are omitted for clarity. Dashed lines represent hydrogen bonds, anion-π and π-π interactions.

The crystal structures of **2**·2(PF_6^-)·0.5(H_2O) shown in Fig. S1 is similar with that of sensor **1**·2(PF_6^-)·(CH_3COCH_3): cave-like conformation of the sensors, hydrogen bonds between a C(2) protons of the benzimidazolium and oxygen atoms (2.25 Å), and anion-π interactions between $[PF_6]^-$ and acridine ring (3.41 Å). Also, for the packing mode, repetitive structure units of the sawtooth-like column were formed by the two types of π-π interactions and were assembled via hydrogen bonds between $[PF_6]^-$ and the adjacent two columns. However, for **2**·2(PF_6^-)·0.5(H_2O), a C(2) proton of the benzimidazolium did not form the obvious hydrogen bond with $[PF_6]^-$, since the shortest F…H distance is 2.80 Å.

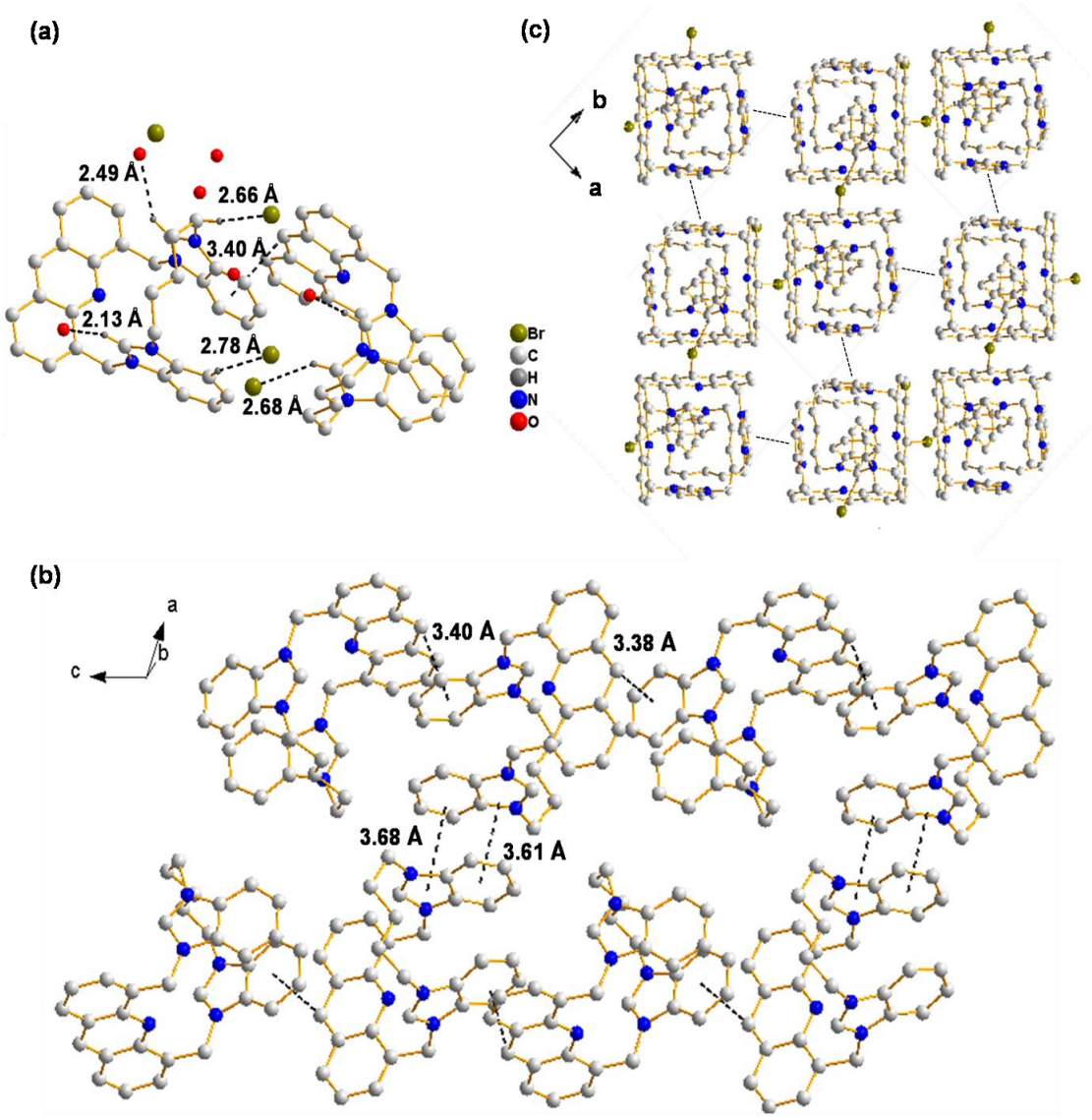

Fig. **S2** Crystal structure (a) and the self-assembly network viewing along b (b) and c (c) axes of **2**·2(Br^-)·3(H_2O). Nonacidic hydrogen atoms, some counterions and solvent molecules are omitted for clarity. Dashed lines represent hydrogen bonds and π-π interactions.

The crystal structure of **2**·2(Br^-)·3(H_2O) was shown in Fig. S2. Two crystallographically distinct conformations with different intramolecular interactions in one unit cell were adopted. In one conformation, two benzimidazolium sites were fully occupied by H_2O molecules. However, in the other, one site was occupied by a H_2O molecule and the other benzimidazolium site preferred to form hydrogen bond with a bromide. The two conformers were connected to each other via intermolecular π-π interaction between an acridine ring and a benzimidazolium, which led to the

formation of an infinite column (Fig. S2b). Fig. S2b and 2c showed two sets of $2\cdot2(Br^-)\cdot3(H_2O)$ arranged in different orientations. The adjacent columns were assembled through π-π interactions between two anti benzimidazoliums (3.61-3.68 Å) (Fig. S2b) and hydrogen bonds with bromide (Fig.S2c), giving rise to the formation of a three-dimensional network by self-assembly.

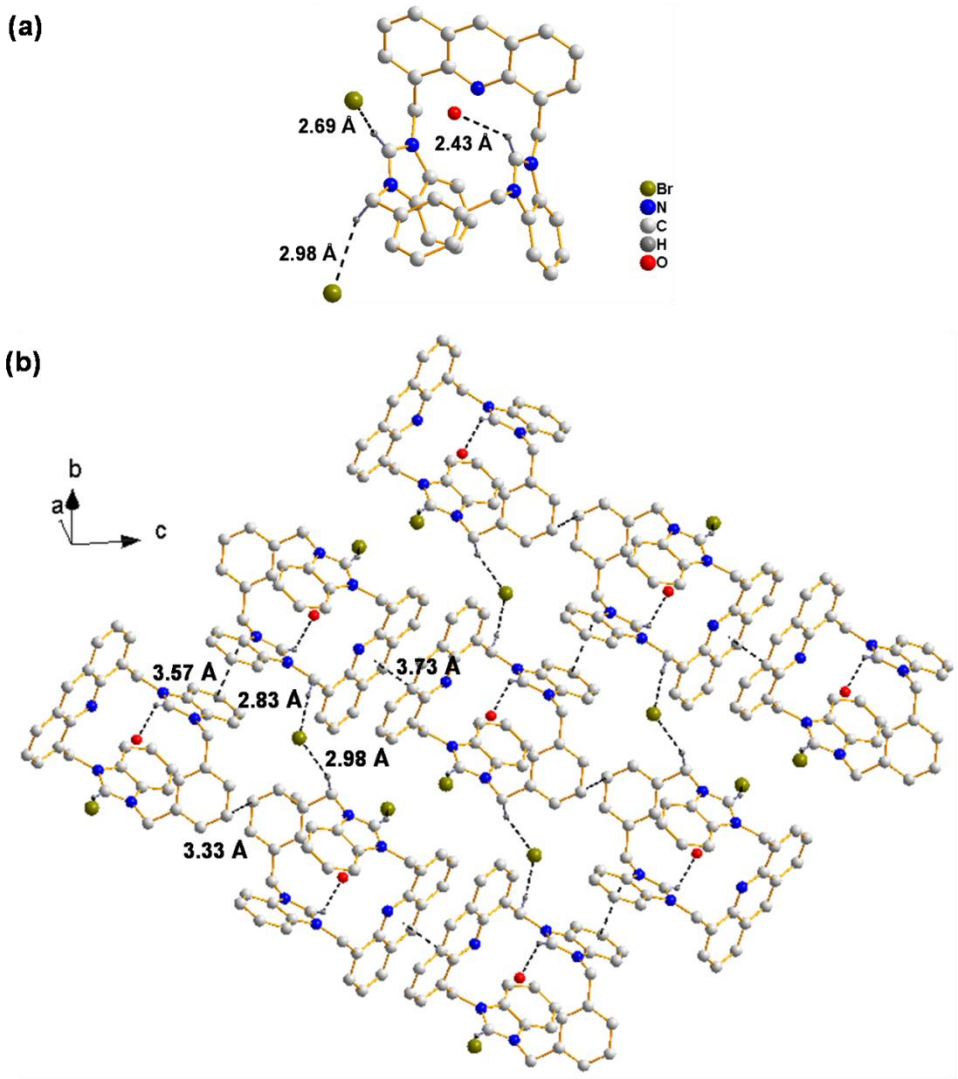

Fig. **S3** Crystal structure (a) and the self-assembly network (b) of **4**·$2(Br^-)\cdot$ (H_2O). Nonacidic hydrogen atoms, some counterions are omitted for clarity. Dashed lines represent hydrogen bonds and π-π interactions.

In the crystal structure of **4**·$2(Br^-)\cdot$ (H_2O) shown in Fig. S3a, a cave-like conformation was also observed. The two directional C(2) protons of the benzimidazoliums formed hydrogen bonds with a bromide counteranion (2.69 Å) and

a oxygen atom of H_2O (2.43 Å) respectively. Another bromide anion formed hydrogen bond with a methylene hydrogen neighboring with benzimidazolium (2.98 Å). A face-to-face π-π interaction between two acridine rings (3.73 Å) and a π-π interaction between two intermolecular benzenes (3.33 Å) keep the three molecules together to form a repetitive structure unit of a column (Fig. S3b). In addition, the two adjacent units were connected to each other by sharing a common bromide anion forming two hydrogen bonds. The combination of the two hydrogen bonds and a π-π interaction between two benzimidazolium in the corresponding two adjacent columns (3.57 Å) led to the formation of a two-dimensional network.

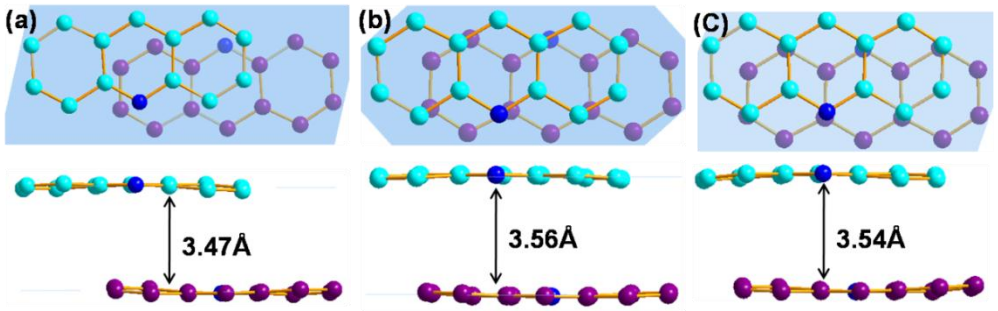

Fig. S4 Comparison on the extent of π-π interactions between two acridine rings of **1**·2(PF_6^-)·(CH_3COCH_3) (a), **2**·2(PF_6^-)·0.5(H_2O) (b) and **4**·2(Br^-)· (H_2O) (c). Arrow lines represent the plane-to-plane distances between two acridine rings.

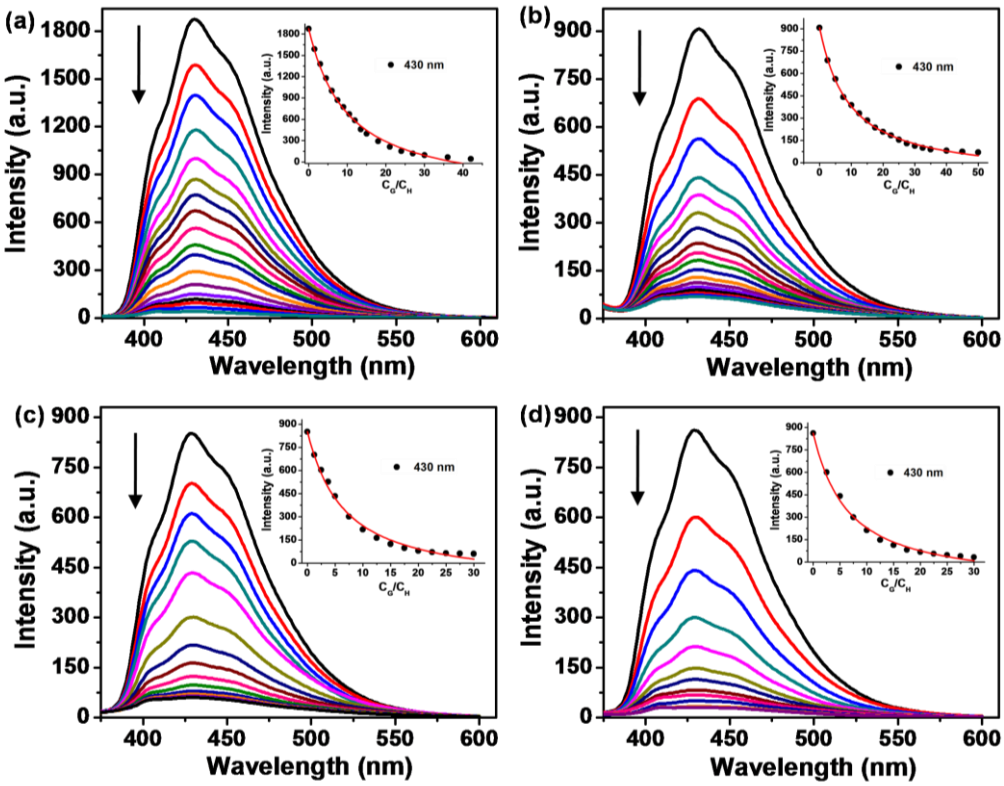

Fig. S5 Fluorescence titrations of 5 μM sensors **1** excited at 362 nm (a), **2** excited at 363 nm (b), **3** excited at 358 nm (c) and **4** excited at 362 nm (d) with TBAF in CH_3CN (excitation and emission slit :5 nm). Inset: intensity developments at 430 nm as a function of added TBAF equivalents.

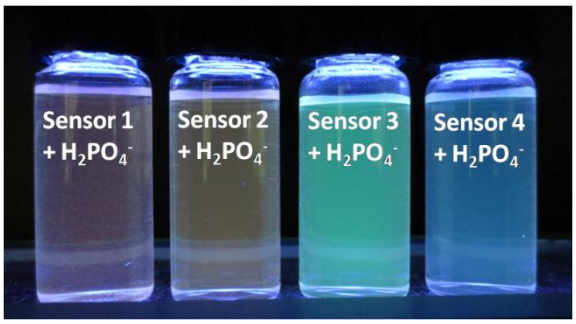

Fig. S6 Fluorescence colors of sensors **1-4** (5 μM) after addition of $TBAH_2PO_4$ two months later (Excitation wavelength of the UV lamp: 365 nm).

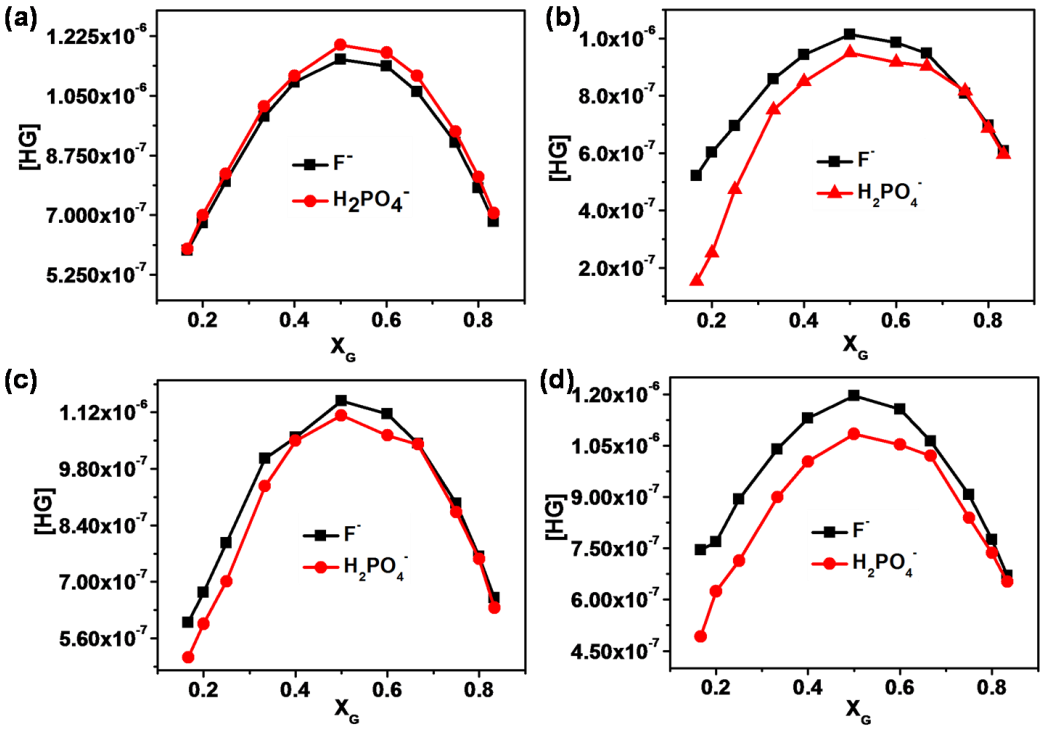

Fig. S7 Fluorescence Job's plots for sensors **1** (a), **2** (b), **3** (c) and **4** (d) with anions.

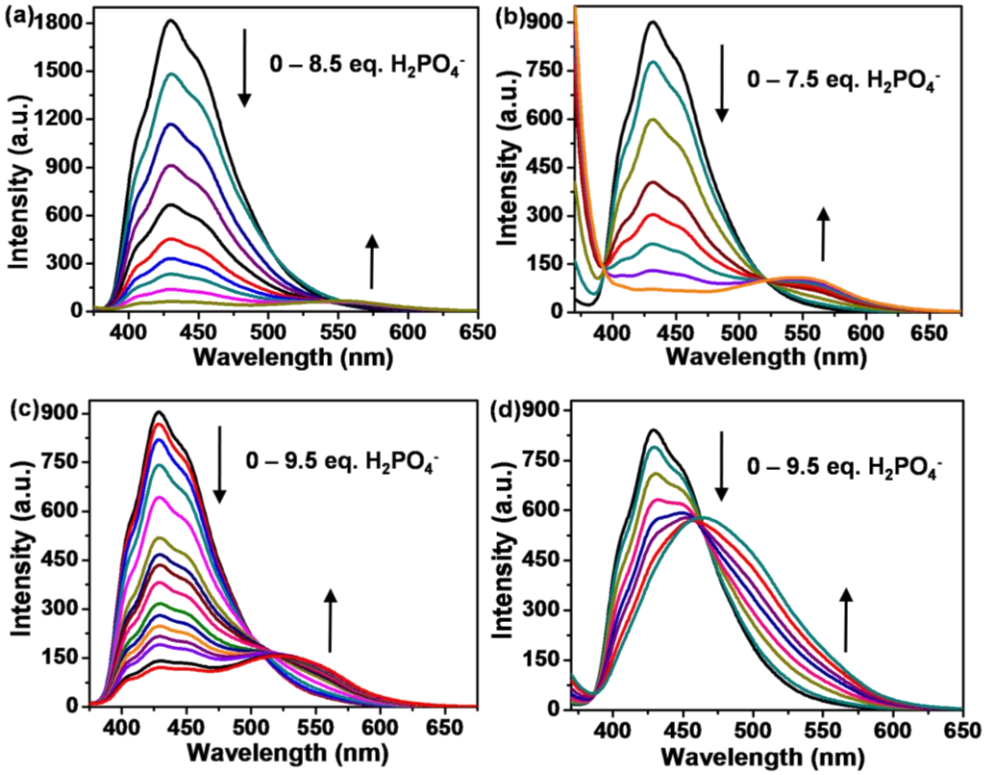

Fig. S8 Fluorescence titrations of 5 μM sensors **1** excited at 362 nm (a), **2** excited at 363 nm (b), **3** excited at 358 nm (c) and **4** excited at 362 nm (d) with $TBAH_2PO_4$ in H_2O-CH_3CN (1:99, v/v) (excitation and emission slit :5 nm).

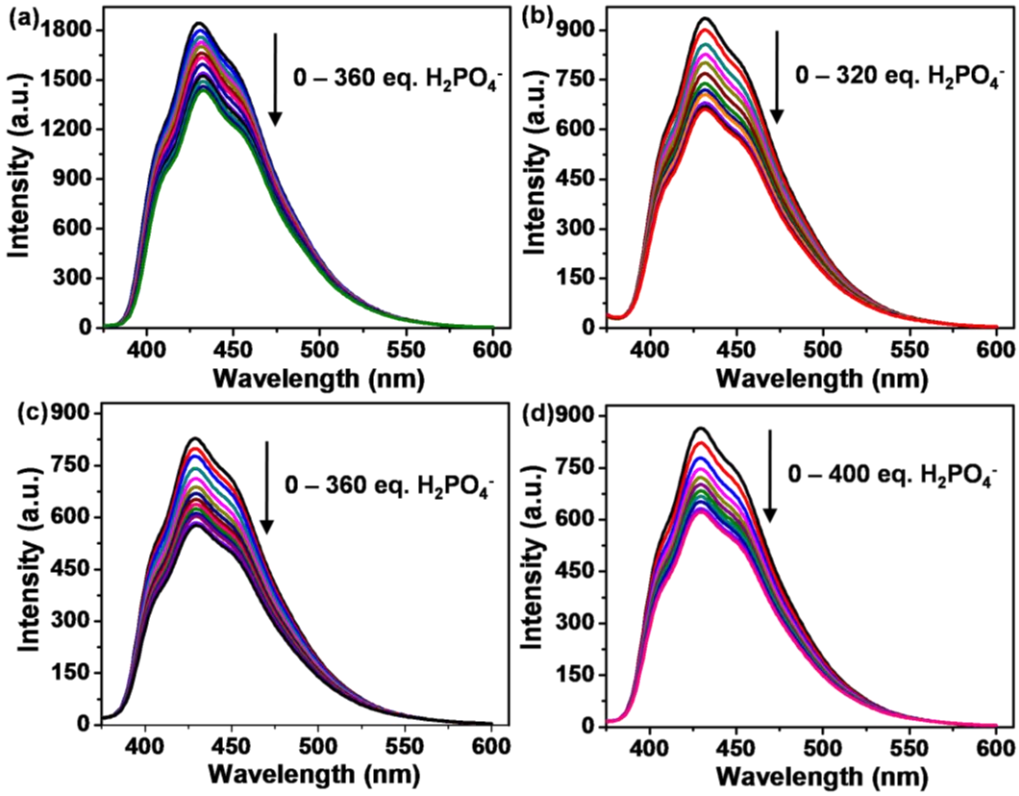

Fig. S9 Fluorescence titrations of 5 μM sensors **1** excited at 362 nm (a), **2** excited at 363 nm (b), **3** excited at 358 nm (c) and **4** excited at 362 nm (d) with $TBAH_2PO_4$ in H_2O-CH_3CN (3:97, v/v) (excitation and emission slit :5 nm).

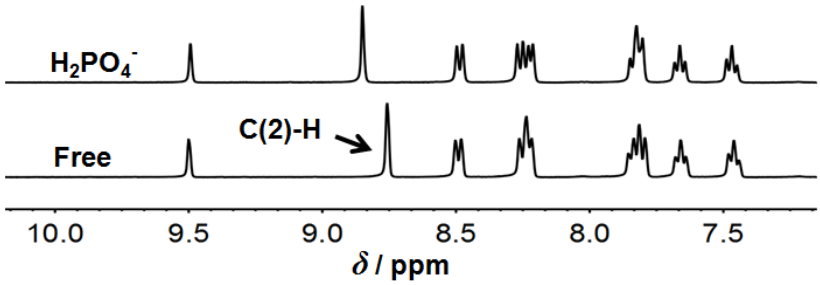

Fig. S10 Partial ^{1}H NMR spectra of sensor **2** (10 mM) in the absence and presence of $TBAH_2PO_4$ (1 equiv.) in DMSO-d_6.

Table S1. Crystal data and refinement for compounds **1**·2PF_6, and **2**·2PF_6.

Compound	**1**·2PF_6	**2**·2PF_6
CCDC	914120	914121
Empirical formula	$C_{36}H_{35}F_{12}N_5OP_2$	$C_{68}H_{56}F_{24}N_{10}OP_4$
M_r	843.63	1609.11
Temperature (K)	296(2)	296(2)
Crystal system	Triclinic	Monoclinic
Space group	$P\bar{1}$	$P2(1)/n$
a/Å	10.958(13)	9.6585(4)
b/Å	11.539(13)	25.7091(12)
c/Å	16.667(19)	14.0835(7)
α/°	75.826(13)	90
β/°	82.501(13)	92.542(2)
γ/°	65.070(12)	90
V/Å^3	1852(4)	3493.7(3)
Z	2	2
Crystal size (mm^3)	0.10 × 0.07 × 0.03	0.10 × 0.07 × 0.03
D_c/g cm^{-3}	1.513	1.530
μ/mm^{-1}	0.216	0.224
F(000)	864	1636
θ range (°)	1.99 - 26.01	1.58 - 28.33
Reflections collected	10277	47852
Unique reflections	7067	8538
GOF on F^2	1.034	1.104
$R_{(int)}$	0.0173	0.0917
R_1 [I >2σ(I)]	0.0744	0.0815
wR_2 (all data)	0.2335	0.2533

Table S2. Crystal data and refinement for compounds **2**·2Br and **4**·2Br.

Compound	**2**·2Br	**4**·2Br
CCDC	914123	914124
Empirical formula	$C_{34}H_{31}Br_2N_5O_3$	$C_{37}H_{29}Br_2N_5O_{0.5}$
M_r	717.46	711.47
Temperature (K)	173(2)	296(2)
Crystal system	Monoclinic	Triclinic
Space group	$P2(1)$	$P\bar{1}$
a/Å	14.481(3)	8.8544(15)
b/Å	13.824(3)	11.0995(19)
c/Å	16.878(3)	16.475(3)
α/°	90	91.233(2)
β/°	109.685(3)	90.453(2)
γ/°	90	105.781(2)
V/Å^3	3181.2(11)	1557.6(5)
Z	4	2
Crystal size (mm^3)	0.65 × 0.65 × 0.25	0.170 × 0.110 × 0.040
D_c/g cm^{-3}	1.498	1.517
μ/mm^{-1}	2.591	2.640
F(000)	1456	720
θ range (°)	1.28 - 27.60	2.25 - 27.55
Reflections collected	22227	9828
Unique reflections	13934	6931
GOF on F^2	1.030	1.082
$R_{(int)}$	0.0562	0.0266
R_1 [I >2σ(I)]	0.0641	R_1 = 0.0630
wR_2 (all data)	0.1815	0.2112

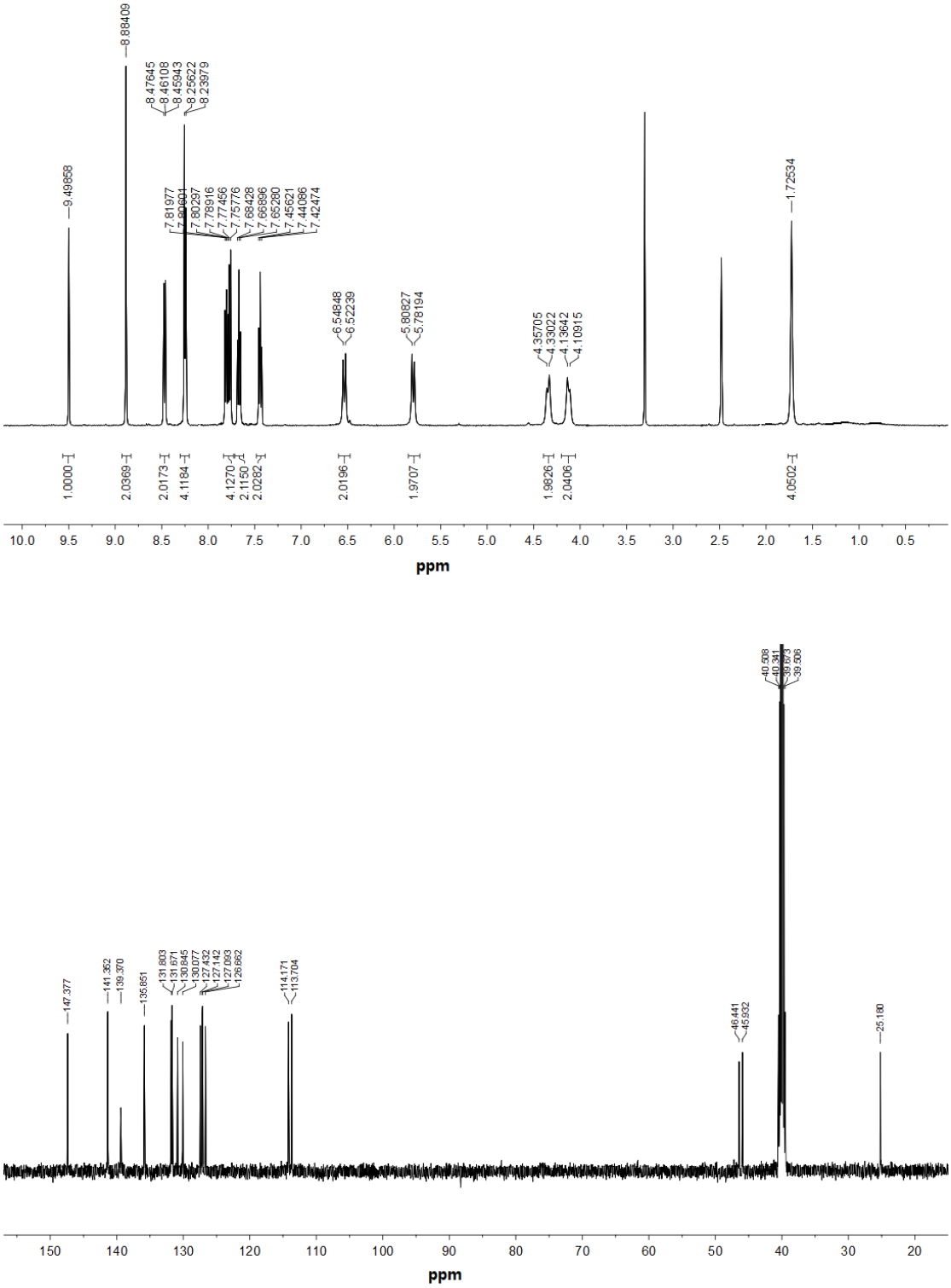

Fig. S11 ^{1}H NMR (top) and ^{13}C NMR (bottom) of sensor **1** in DMSO-d_6.

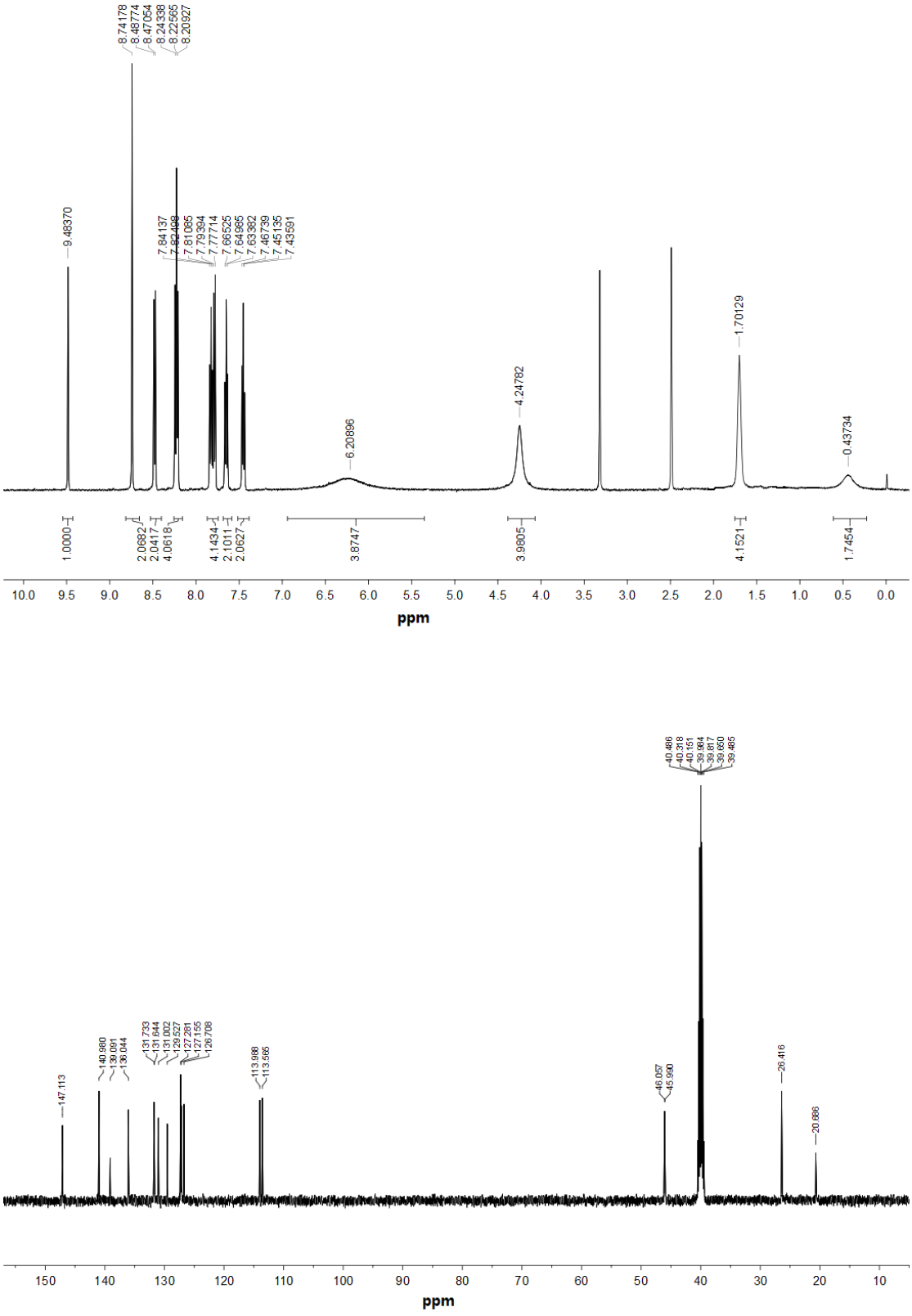

Fig. S12 ^{1}H NMR (top) and ^{13}C NMR (bottom) of sensor **2** in DMSO-d_6.

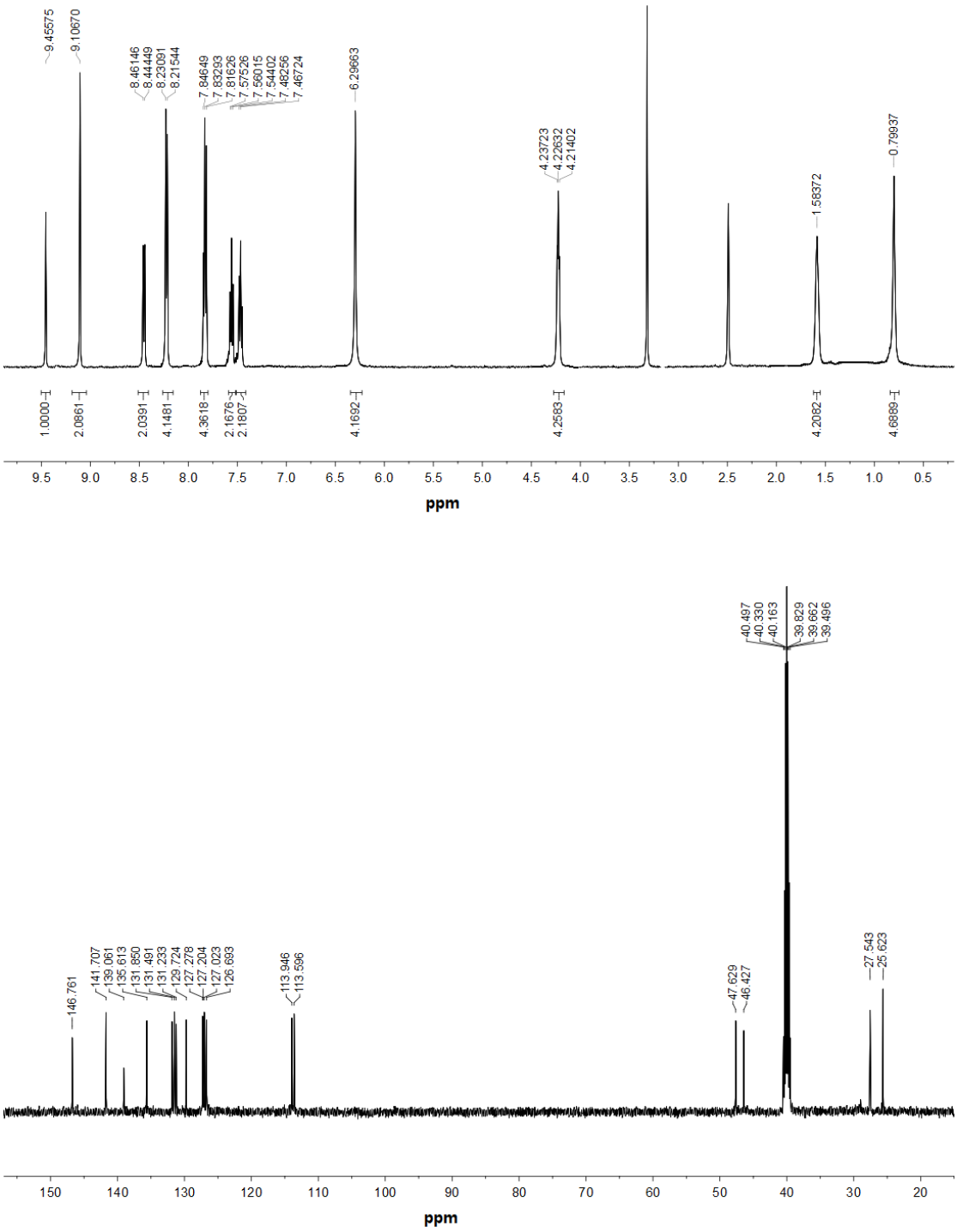

Fig. S13 ^{1}H NMR (top) and ^{13}C NMR (bottom) of sensor **3** in DMSO-d_6.

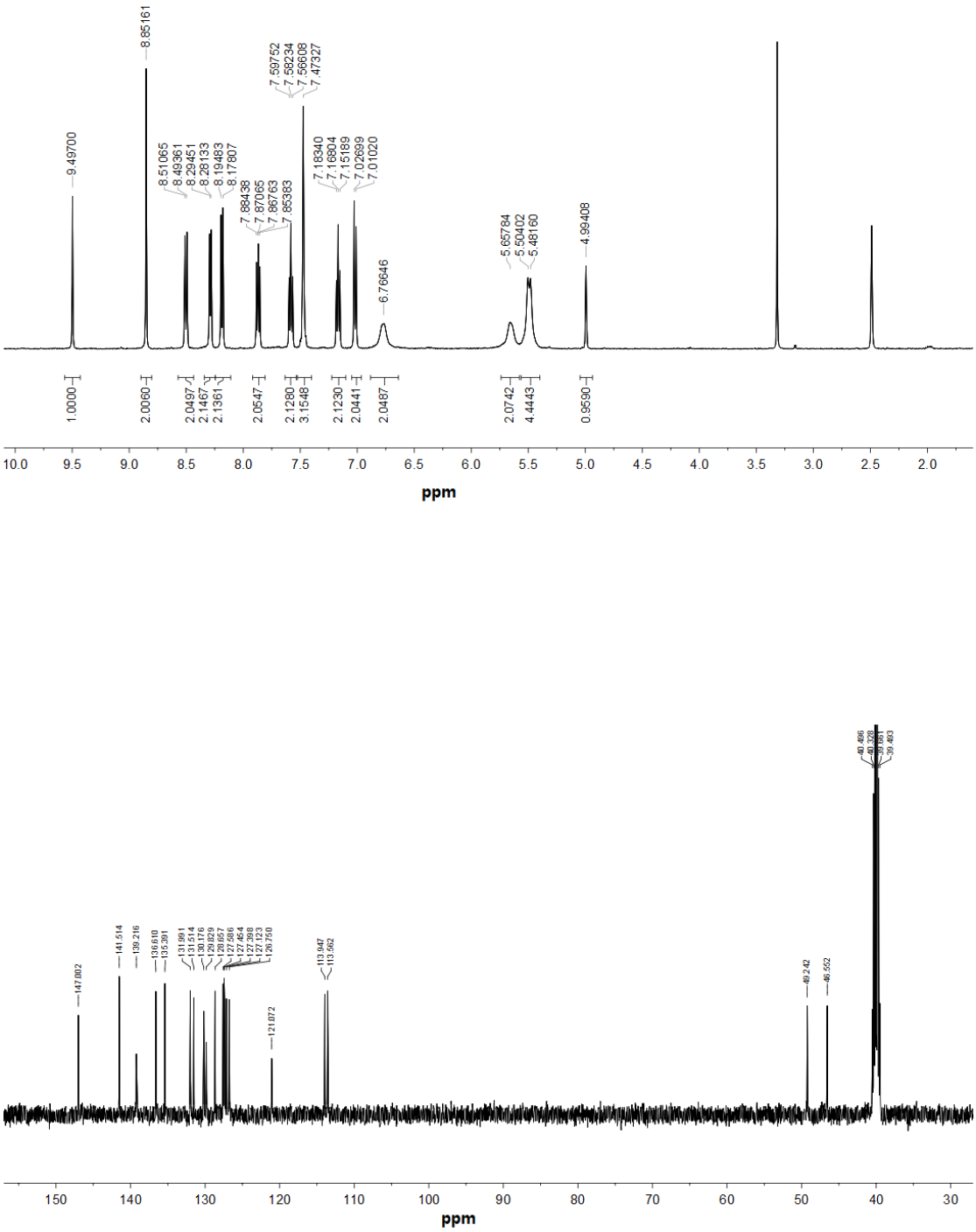

Fig. S14 ^{1}H NMR (top) and ^{13}C NMR (bottom) of sensor **4** in DMSO-d_6.